Carbohydrate Polymers 102 (2014) 691–698

Contents lists available at ScienceDirect

Carbohydrate Polymers

journal homepage: www.elsevier.com/locate/carbpol

Magnetic core–shell chitosan nanoparticles: Rheological characterization and hyperthermia application

Vanessa Zamora-Mora[a], Mar Fernández-Gutiérrez[a,c], Julio San Román[a,c], Gerardo Goya[b], Rebeca Hernández[a,*], Carmen Mijangos[a]

[a] Instituto de Ciencia y Tecnología de Polímeros (CSIC), c/Juan de la Cierva, 3, 28006 Madrid, Spain
[b] Instituto de Nanociencia de Aragón, Universidad de Zaragoza, Mariano Esquillor, 50018 Zaragoza, Spain
[c] CIBER-BBN, Ebro River Campus Building R&D Block 5, Floor 1, Poeta Mariano Esquillor s/n, 50017 Zaragoza, Spain

ARTICLE INFO

Article history:
Received 21 August 2013
Received in revised form 17 October 2013
Accepted 31 October 2013
Available online 8 November 2013

Keywords:
Chitosan
Sodium tripolyphosphate
Core–shell nanoparticles
Magnetic hyperthermia

ABSTRACT

Stabilized magnetic nanoparticles are the subject of intense research for targeting applications and this work deals with the design, preparation and application of specific core–shell nanoparticles based on ionic crosslinked chitosan. The nanometric size of the materials was demonstrated by dynamic light scattering (DLS) and field emission scanning electron microscopy (FESEM) that also proved an increase of the size of chitosan nanoparticles (NPs) with the magnetite content. Steady oscillatory rheology measurements revealed a gel-like behavior of aqueous dispersions of chitosan NPs with concentrations ranging from 0.5% to 2.0% (w/v). The cytotoxicity of all the materials synthesized was analyzed in human fibroblasts cultures using the Alamar Blue and lactate dehydrogenase (LDH) assays. The measured specific power absorption under alternating magnetic fields (f = 580 kHz, H = 24 kA/m) indicated that magnetic core–shell chitosan NPs can be useful as remotely driven heaters for magnetic hyperthermia.

1. Introduction

Chitosan, a cationic polysaccharide obtained by the thermo-alkaline N-deacetylation of chitin, is the second-most abundant naturally occurring amino polysaccharide offering high biocompatibility (Muzzarelli, 2011; Muzzarelli et al., 2012). Chitosan has attracted intense attention as an important biopolymer to effectively stabilize colloidal dispersions of superparamagnetic iron oxide nanoparticles, conferring them an increased biocompatibility and chemical functionality (Dias, Hussain, Marcos, & Roque, 2011; Nicolás et al., 2013). These materials find applications in magnetic hyperthermia treatment of cancer, a promising approach to cancer therapy in which the temperatures of tumors are increased to 41–46 °C to induce apoptosis of the cells (Jordan, Scholz, Wust, Fähling, & Roland, 1999; Laurent, Dutz, Häfeli, & Mahmoudi, 2011). This therapy involves the introduction of ferromagnetic or superparamagnetic nanoparticles (mainly magnetite, Fe_3O_4) into the tumor tissue and then irradiation with an alternating magnetic field (AMF). The particles transform the energy of the AMF into heat by different physical mechanisms, and the transformation efficiency strongly depends on the frequency of the external field (Gellermann et al., 2006) as well as the nature of the particles such as particle size (Goya et al., 2008) or surface modification (Gupta & Gupta, 2005).

Magnetic hydrogels, a combination of hydrogels with micro- and/or nanomagnetic particles (e.g., γ-Fe_2O_3, Fe_3O_4, $CoFe_2O_4$) have been implemented as materials able to heat up target tumors remotely through an external magnetic field (Hernandez, Sacristán, Asi'n et al., 2010; Li et al., 2013). We reported on the employment of chitosan as a template for the oxidation of iron cations to yield simultaneously iron oxide nanoparticles and the formation of a chitosan gel (Hernández et al., 2009). These materials show a high quality thermal response in the presence of an AMF which makes them potential candidates for applications in magnetic hyperthermia (Hernandez, Sacristán, Asi'n et al., 2010).

In recent years, the preparation of magnetic chitosan NPs has attracted a great attention in order to develop thermoseeds for magnetic hyperthermia that can also be injected for localized therapy as in the case of ferrofluids (Jordan et al., 2001; Kim, Kim, Kim, & Lee, 2008; Zhao, Wang, Zeng, Xia, & Tang, 2009). Chitosan-Fe_3O_4 NPs can be prepared in situ with tiny pools of water-in-oil microemulsion containing chitosan and ferrous salt as micro-reactors by adding the basic precipitant, NaOH, into the micro-emulsion (Zhi, Wang, Lu, Ma, & Luo, 2006). The encapsulation of preformed iron oxide nanoparticles can be stabilized by crosslinking chitosan with glutaraldehyde (Jiang, Long, Huang, Xiao, & Zhou, 2005) or tripolyphosphate salts (TPP). Crosslinking of chitosan with TPP constitutes a mild and efficient method to

* Corresponding author. Tel.: +34 915 622 900; fax: +34 915 644 853.
E-mail address: rhernandez@ictp.csic.es (R. Hernández).

0144-8617/$ – see front matter © 2013 Elsevier Ltd. All rights reserved.
http://dx.doi.org/10.1016/j.carbpol.2013.10.101

achieve chitosan NPs (Calvo, Remuñán-López, Vila-Jato, & Alonso, 1997; Goycoolea, Lollo, Remuñán-López, Quaglia, & Alonso, 2009). Sodium tripolyphosphate (TPP) is a polyanion categorized as being GRAS (generally recognized as safe) by the FDA (Food and Drug Administration) (Ur-Rehman, Tavelin, & Gröbner, 2011). It is known that the chitosan particles are formed mainly through the electrostatic interaction between positively charged chitosan and negatively charged TPP molecules. The understanding of the macroscopic rheological properties of the resulting aqueous colloidal dispersions is of paramount importance for the design of biomedical applications (Guvendiren, Lu, & Burdick, 2012). In a recent report, the packing of chitosan NPs to form microgels from aqueous suspensions was ascertained through rheological measurements for samples with different particle sizes obtained by varying the chitosan to TPP ratio (Li & Huang, 2012).

In this paper, the encapsulation of Fe_3O_4 nanoparticles into chitosan NPs crosslinked with TPP is described and the rheological properties of the aqueous dispersions were investigated through dynamic rheological measurements. The rheological characterization will allow determining the structural organization of these materials by relating their linear viscoelastic properties to their properties in dispersion by means of scaling laws (Echeverria, Peppas, & Mijangos, 2012; Hernandez, Sacristan, Nogales et al., 2010). The work extends to a study on remote heating by a magnetic field and the analysis of cytotoxicity to evaluate the application of the materials obtained for magnetic hyperthermia.

2. Materials and methods

2.1. Materials

Chitosan with a deacetylation degree (DD) of 65% and molecular weight (M_w) of 362 kDa was supplied by Laboratorio de Polímeros, Universidad Nacional de Costa Rica. This chitosan was isolated from shrimp's shell (*Heterocarpus vicarious*).

Acetic acid (Aldrich) and sodium tripolyphosphate (Aldrich) were used as received. Oleic-acid-coated iron oxide nanoparticles dispersed in water as a ferrofluid (density = 1.08 g/mL), NGAP FeO-05#4, were provided by Nanogap subnmparticles, Spain. According to the manufacturer, the crystalline form is magnetite, Fe_3O_4 and the average size of nanoparticles is 18.55 ± 2 nm. Milli-Q (18.3 MΩ) water was used in all experiments.

2.2. Preparation of chitosan–sodium tripolyphosphate (CS + TPP) nanoparticles

CS + TPP nanoparticles were prepared as reported elsewhere (Calvo et al., 1997). Briefly, 0.5% (w/v) chitosan stock solutions were prepared by dissolving the appropriate chitosan weight into a 1% (v/v) acetic solution. Sodium tripolyphosphate (TPP) was dissolved in Milli-Q water to a final concentration of 0.5% (w/v). CS + TPP nanoparticles were formed by dropwise addition of TPP solution into a chitosan stock solution under severe magnetic stirring. A chitosan to TPP mass ratio of 5 was chosen based on previous studies (Li & Huang, 2012). Finally, aqueous dispersions of CS + TPP nanoparticles were centrifuged at 5000 rpm for 20 min and the supernatant was separated and subjected to freeze-drying.

The crosslinking degree of CS + TPP nanoparticles was 68% as determined by the ninhydrin test. Ninhydrin is extensively used in the analytical determination of amino acids and related structures because it can react with a variety of primary and secondary amines producing *Ruhemann* purple color. This product has a maximum absorbance at 570 nm (Wu, Hussain, & Fassihi, 2005).

2.3. Preparation of Fe_3O_4–chitosan nanoparticles (NP + Fe)

Fe_3O_4 chitosan nanoparticles (NP + Fe) with three different Fe_3O_4 contents were prepared based on the following steps: firstly, a determined amount of ferrofluid was dispersed in 5 mL of water to yield various concentrations of Fe_3O_4 nanoparticles (0.5%, 2.0% and 5.0%, w/v). The resulting ferrofluid was added under vigorous stirring to 30 mL of a chitosan solution in acetic acid (0.5%, w/v, pH = 3.5) in a N_2 atmosphere. Secondly, an aqueous TPP solution (0.5%, w/v, pH = 9.2) was dropped into the chitosan solution containing magnetite nanoparticles (final pH ~ 4, for all the samples). This step allowed encapsulating magnetite nanoparticles into CS + TPP nanoparticles. Finally, aqueous dispersions of NP + Fe nanoparticles were centrifuged at 5000 rpm for 20 min and the supernatant was separated and subjected to freeze-drying.

The magnetite concentration in the chitosan nanoparticles was determined through UV spectroscopy. Samples were digested in HNO_3 and HCl 6 M and iron concentration was measured spectrophotometrically at the λ_{max} of 478 nm.

2.4. Dynamic light scattering (DLS) and zeta potential

Dynamic light scattering (DLS, Malvern Nanosizer Nano S) was employed for the determination of electrophoretic mobility and hydrodynamic diameter of chitosan nanoparticles dispersed in Mili-Q water at 25 °C, the resulting pH of the dispersions was 4.5. For hydrodynamic diameter determinations, a backscattering detection angle of 173° was employed. The electrophoretic mobility was transformed into zeta potential using the Smoluchowski equation. All measurements were repeated three times and the average of three runs was taken as the result.

2.5. Morphology studies

Micrographs of the samples were taken using a FESEM Hitachi model SU8000 HRSEM used in the TE (electron transmission) detector bright field mode and SE operated at 0.5–30 kV. One drop corresponding to aqueous dispersions of each of the samples under study was deposited on the Formvar carbon-coated Cu grid.

2.6. Fourier-transform infrared spectroscopy (FT-IR)

Fourier-transform infrared spectroscopy was performed on a Perkin Elmer spectrometer. The pellets were prepared on a KBr press. The spectra were scanned over the wave number range of 4000–450 cm^{-1} at a resolution of 2 cm^{-1}.

2.7. Rheology

Dynamic oscillatory measurements were performed in a AR-G2 rheometer (TA Instruments, USA). The geometry used was 60 mm acrylic parallel plates. Samples under study were dispersed in ultrapure water at concentrations ranging from 0.5% to 2.0% (w/v). This range was chosen because concentrations higher than 2.0% w/v did not allow the homogeneous dispersion of the samples in water and lower than 0.5% w/v did not allow the rheological characterization due to the torque limit. Strain sweep tests at a constant, nondestructive 0.5 Hz frequency were carried out. All measurements were done at room temperature.

2.8. Cell culture conditions

The biological response to the materials was tested with fibroblasts of human embryonic skin (HFB, Innoprot). The culture medium was Dulbecco's modified Eagle's medium enriched with 4500 mg/mL of glucose (DMEM, Sigma) and supplemented with

Table 1
Experimental concentrations (mg/mL) employed in cytotoxicity Alamar Blue assay.

D1	2.50 mg/mL	D6	0.078 mg/mL
D2	1.250 mg/mL	D7	0.039 mg/mL
D3	0.625 mg/mL	D8	0.020 mg/mL
D4	0.313 mg/mL	D9	0.010 mg/mL
D5	0.156 mg/mL	D10	0.005 mg/mL
		D11	0.002 mg/mL

10% fetal bovine serum (GIBCO, Life Technologies, Spain) 200 mM L-glutamine, 100 units/mL penicillin and 100 mg/mL streptomycin, modified with HEPES (Sigma, Spain).

The culture medium was changed at selected time intervals with little disturbance to culture conditions. Cells without treatment were used as a negative control. NP + Fe samples were dispersed in fresh medium without phenol red at different concentrations. Samples were sterilized with a UV lamp (HNS OSRAM, 263 nm, 3.6 UVC/W) at a power of 11 W for 4 h. Sterile plastic was supplied by Sasrtedt, Spain.

2.9. Cytotoxicity analysis

2.9.1. Alamar Blue assay

For determination of cytotoxicity, the Alamar Blue (AB was provided by Serotec, Spain) assay was performed. Cells were seeded at a density of 8×10^4 cells/mL in complete medium in a sterile 96-well culture plate and incubated to confluence.

After 24 h of incubation, the medium was replaced with the corresponding aqueous dispersions of NP + Fe samples at different concentrations (Table 1) and incubated at 37 °C in humidified air with 5% CO_2 for 24 h. After this time, a solution of AB was prepared in warm medium without phenol red and the plates were incubated at 37 °C for 4 h. Finally, fluorescence was measured with a Biotek Synergy HT detector using an emission wavelength of 590 nm and an excitation wavelength of 530 nm.

Cell viability (CV) was calculated with the following equation:

$$CV = 100 \times \left(\frac{FD_s - FD_B}{FD_C - FD_B} \right)$$

where FD_S, FD_B, and FD_C are the fluorescence density of the AB for the sample (S), blank (B) (culture medium without cells), and control (C).

2.10. Lactate dehydrogenase assay

Lactate dehydrogenase (LDH), which is a soluble cytosolic enzyme present in most eukaryotic cells, releases into culture medium upon cell death due to damage of plasma membrane. The increase of the LDH activity in culture supernatant is proportional to the number of lysed cells.

We employed LDH cytotoxicity assay kit (Innoprot, Spain). LDH catalyses the reduction of NAD+ to NADH in the presence of L-lactate, while the formation of NADH can be measured in a coupled reaction in which the tetrazolium salt is reduced to a red formazan product. The amount of the highly colored and soluble formazan can be measured at 490 nm spectrophotometrically.

The protocol is analogous to the Alamar Blue assay. The concentrations employed for the preparation of aqueous dispersions of NP + Fe samples were 1.0 and 0.05 mg/mL.

2.11. Specific power absorption experiments

The specific power absorption (SPA) of the aqueous dispersions of NP + Fe samples at a 5.0% w/v concentration was measured with a commercial AC field applicator (DM100 by nB nanoscale Biomagnetics, Spain) working at f = 580 kHz and 24 kA/m (≈300 Oe).

Table 2
Mean particle size, zeta potential and magnetite concentration determined for all the samples under investigation.

Sample	Magnetite concentration* (mg/mL)	Mean particle size (nm)	Zeta potencial (mV)
CS + TPP	0	140 ± 1	63.4 ± 0.8
NP + Fe 1.0%	1.0	192 ± 2	57.2 ± 2.0
NP + Fe 3.2%	3.2	205 ± 3	59.3 ± 0.8
NP + Fe 5.6%	5.6	259 ± 1	57.9 ± 6.6

Data shown are the mean ± standard deviation.
* Determined through UV–vis spectroscopy.

Experiments were carried within a thermally-insulated working space of about 1 cm^3, using a closed container of 1.0 mL volume conditioned for measurements in liquid phase.

3. Results and discussion

3.1. Preparation and characterization of NP + Fe samples

NP + Fe samples were synthesized by the ionic crosslinking reaction between the protonized ammonium groups of chitosan and the tripolyphosphate anions of TPP in the presence of the ferrofluid. An electrostatic interaction is established in the reaction between chitosan and TPP, enabling the encapsulation of an amount of magnetite ferrofluid (negative surface charge) within a positive matrix (chitosan) and using TPP as ionic crosslinking agent with negative charge of its phosphate groups (Rodrigues, Costa, & Grenha, 2012). The acid media guarantees the protonation of the amino groups of chitosan.

Table 2 reports the mean particle size, the zeta potential and the magnetite concentration determined through UV spectroscopy for all the samples under investigation.

Samples with magnetite are denoted as NP + Fe 1.0%, NP + Fe 3.2% and NP + Fe 5.6% where the numbers denote the iron content determined through UV–vis spectroscopy. As can be observed, magnetite encapsulation gives rise to an increase in the size of NP + Fe samples with respect to the CS + TPP sample. Furthermore, NP + Fe samples show an increase in their particle size from 192 to 259 nm as magnetite content is increased from 1.0% to 5.6%. This result might be attributed to the fact that magnetite nanoparticles are subjected to Van der Waals forces and magnetic dipole-dipole interactions generated from residual magnetic moments (Zhu, Yuan, & Liao, 2008) that together may produce an increase in the particle size.

The positive zeta potential encountered for the CS + TPP sample (63.4 ± 0.8 mV) was due to the protonated ammonium groups in the acidic environment that resulted from the dispersion in Mili-Q water (pH 4.5). The zeta-potential of all the NP + Fe samples remained positive in the range of 57–63 mV, in close agreement with previous reports (Li & Huang, 2012). It is important to note that the zeta-potencial corresponding to the commercial ferrofluid is negative (−75.8 ± 3.2 mV) which suggest its encapsulation into the chitosan NPs as it will be ascertained through microscopy images shown in the next section.

Fig. 1 shows FT-IR spectra of pure TPP, chitosan, CS + TPP and NP + Fe 3.2%. In the TPP spectrum, the following characteristic bands can be observed: 1218 cm^{-1} (P═O stretching), 1143 cm^{-1} (symmetric and antisymmetric stretching vibrations in PO_2 group), 1069 cm^{-1} (symmetric and antisymmetric stretching vibrations in PO_3 group), 898 cm^{-1} (antisymmetric stretching of the P—O—P bridge). The characteristic vibrational absorption bands observed in the chitosan spectrum (Fig. 1B) are the band at 1593 cm^{-1} corresponding to the N—H bending vibration overlapping the amide II vibration and that at 1652 cm^{-1} that corresponds to the amide I vibration (Lawrie et al., 2007). Absorption bands at 1153 cm^{-1} (antisymmetric stretching of C—O—C), 1089 and 1033 cm^{-1} (skeletal

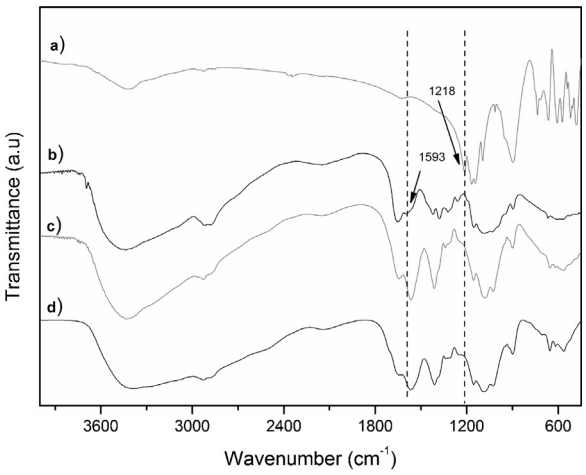

Fig. 1. FT-IR spectra corresponding to (a) TPP, (b) chitosan, (c) NP + Fe 3.2% and (d) CS + TPP.

vibrations involving CO stretching) are characteristic of the chitosan saccharide structure (Pawlak & Mucha, 2003).

FT-IR spectroscopy is an appropriate technique to study the chitosan-TPP interaction, since a shift in the δ_{NH_3} vibration may be expected when NH_3^+ groups interact electrostatically with the negatively charged sites of the TPP as previously shown for chitosan nanocomposites (Darder, Colilla, & Ruiz-Hitzky, 2003). In fact, a shift of the δ_{NH_3} band toward a lower frequency is observed in the spectra corresponding to CS + TPP and NP + Fe 3.2 spectra for which the band at 1593 cm^{-1} (shown in Fig. 1) shifts to 1570 and 1568 cm^{-1}, respectively. The shift of the band position and the increase of intensity observed could be attributed to the ionic crosslinking between the NH_3^+ from chitosan and the $P_3O_{10}^{5-}$ from TPP (Darder, Colilla, & Ruiz-Hitzky, 2005). In both spectra, a new band at 1218 cm^{-1} appears that can be assigned to P=O stretching vibrations in phosphate ions (shown in Fig. 1). In the spectrum corresponding to NP + Fe 3.2%, it is not possible to observe the characteristic band of iron oxide centered at 563 cm^{-1}(Zhang et al., 2010) because of the overlapping with characteristic bands from chitosan and TPP.

Fig. 2 shows representative FESEM micrographs corresponding to the sample NP + Fe 5.6% obtained by bright field (BF) (Fig. 2a) and SE image (Fig. 2b).

Bright field image allows corroborating the core–shell encapsulation of magnetite within a layer of chitosan that constitutes the shell. SE image taken on the same spot shows the smooth surface of the chitosan NPs which confirms the magnetite encapsulation with a core–shell morphology (Doiron, Homan, Emelianov, & Brannon-Peppas, 2009).

A schematic representation of the preparation of NP + Fe samples is shown in Fig. 3. As can be observed, the crosslinking of TPP and chitosan in the presence of magnetite gives rise to its encapsulation into the chitosan NPs. Size measurements performed on images obtained through bright field microscopy allows estimating that the magnetic core size is in the range 75–220 nm whereas the shell size varies in the range 21–39 nm.

3.2. Rheological study of aqueous dispersions of NP + Fe nanoparticles

Recent results regarding the rheological behavior of aqueous dispersions of poly (acrylamide-acrylic acid) microgels outlined their macroscopic elasticity showing that the material behaves as a colloidal gel (Echeverria, Peppas, & Mijangos, 2012). Taking into account these results, the rheological characterization of aqueous colloidal dispersions is of paramount importance, and allows anticipating their behavior under certain conditions of shear.

Shear-thinning of a colloidal suspension could enable a more homogeneous and easy delivery of the material to the body in the case of injectable materials (Guvendiren et al., 2012). Moreover, the recovery of the elastic properties immediately after injection may prevent the flow of the colloidal solution and facilitate that the material remains on the target site (Yan et al., 2012). A possible recovery of the elastic properties after shear-thinning was explored by comparing up and down strain sweeps carried out on NP + Fe 3.2% sample. Fig. 4a shows that as the strain diminishes, immediately after shear thinning, a significant recovery of the elastic properties is observed and the sample recovered almost the initial elastic modulus.

The results corresponding to the strain sweeps carried out on the sample NP + Fe3.2% at different concentrations of the dispersion in water ranging from 0.5% (w/v) to 2.0% (w/v) are depicted in Fig. 4b. For all the concentrations studied, the sample display a linear viscoelastic regime characterized by the independence of G' and G'' on the strain and yield up to a critical shear amplitude, γ_0, above which the sample shows a viscoelastic liquid-like behavior followed by apparent shear-thinning.

Shear-thinning could be attributed to the breaking apart of clusters formed among the particles at high shear amplitude. The increase in γ_0 that occurs when the concentration of the dispersion increases from 0.5% (w/v) to 2.0% (w/v) indicates that clusters are less dense at lower dispersion concentrations. Therefore, once some inter-cluster bond that keep the interconnected network solid break, the sample may flow. The increase in the concentration of the dispersion gives an increase of the corresponding elastic

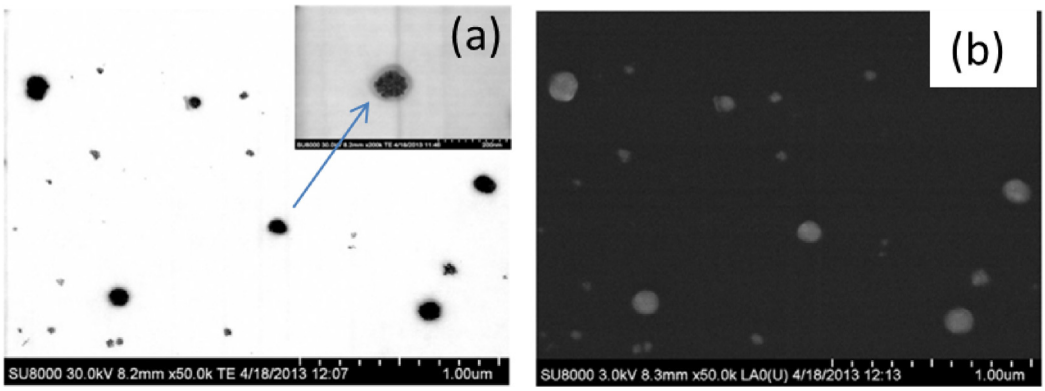

Fig. 2. Representative micrograph corresponding to NP + Fe 5.6% nanoparticles obtained through FESEM microscopy, corresponding to (a) bright field and (b) SE image. The inset in Fig. 2a shows a magnification of a core–shell chitosan nanoparticle.

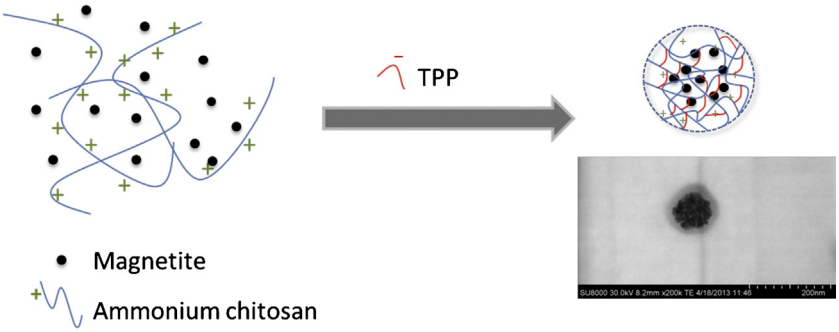

Fig. 3. Schematic representation of the preparation of NP + Fe nanoparticles. (A) Bright field FESEM microscopy obtained for the sample NP + Fe 5.6% at a high magnification is also shown in figure.

modulus which could be associated to the intrinsic elastic properties of the different nanoparticles or the clusters.

Similar conclusions can be reached from the strain sweeps corresponding to CS + TPP, NP + Fe 1.0% and NP + Fe 5.6% samples dispersed at different concentrations ranging from 0.5% (w/v) to 2% (w/v) in water. For CS + TPP sample, it was not possible to measure concentrations lower than 1.0% (w/v) due to the inertia of the measurement (supplementary information).

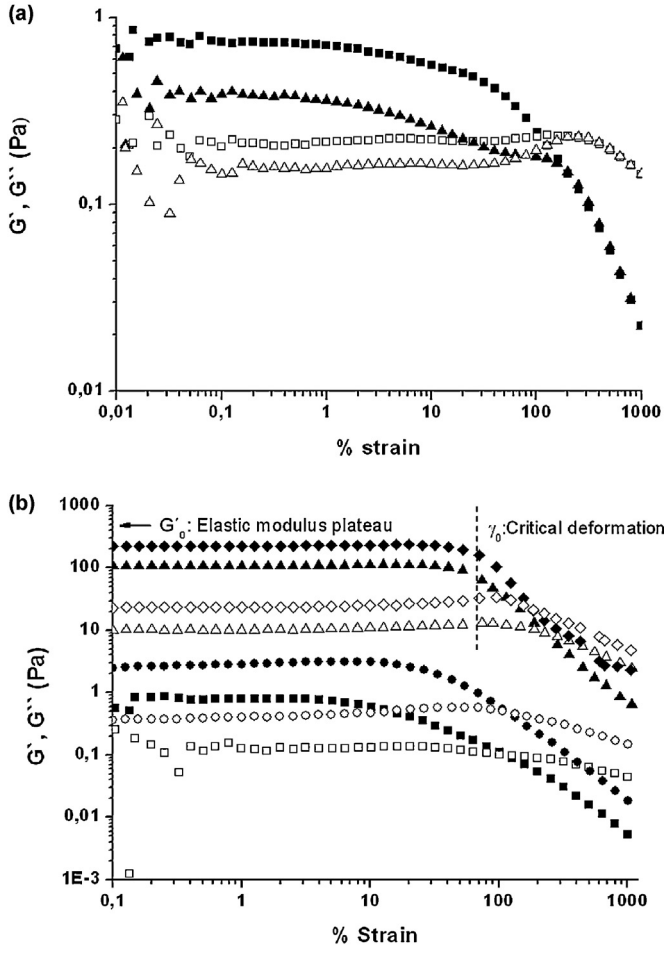

Fig. 4. (A) Evolution of the elastic modulus (full symbol) and viscous modulus (empty symbol) as a function of strain for an aqueous dispersion (1%, w/v) of the sample NP + Fe 3.2%. First strain sweep (square) and second strain sweep (triangle). (B) Evolution of the elastic modulus (full symbol) and viscous modulus (empty symbol) as a function of strain for aqueous dispersions of the sample NP + Fe 3.2% at different concentrations: 0.5%, w/v (square), 1%, w/v (circle), 1.5%, w/v (triangle), and 2%, w/v (diamond).

An important parameter that determines the elasticity encountered in dispersions of chitosan NPs is the presence of interactions among particles which may lead to an increase in the elastic modulus. These interactions are responsible for the solid behavior observed in many colloidal dispersions (Pham, Egelhaaf, Pusey, & Poon, 2004; Pham et al., 2002). As a consequence, these systems transform from solid-to-liquid like at increasing applied stress, they yield (Pham et al., 2006).

Results obtained from strain sweeps carried out at different concentrations show that both elastic modulus and critical deformations presented dependence with the concentration. These results indicate the occurrence of an aggregating system that may form a gel which can be studied by applying a fractal analysis. In this way the colloidal gel structure can be related to the rheological properties based on scaling laws (Echeverria, López, & Mijangos, 2009).

A representation of the plateau values of G_0 and γ_0 already determined from the strain sweep experiments are plotted as a function of concentration in double-logarithmic form in Fig. 5a and b, respectively.

The elastic modulus plateau increased as a function of the concentration of the dispersion for all the samples. The same behavior was observed for the critical deformation which indicates that as the concentration of the dispersion increases, it is necessary to apply more deformation to break the clusters. When samples with different magnetite contents are compared at the same concentration of the dispersion, an increase of the elastic modulus of the samples with magnetite is observed with respect to the CS + TPP samples.

Both the elastic modulus and the critical deformation can be linearly fitted to relations of the type:

$$G_0' \approx \varphi^A$$

$$\gamma_0 \approx \varphi^A$$

where φ is the volume fraction and the exponents, A and B are the slopes corresponding to the fitting lines.

According to the Wu and Morbidelli model (Wu & Morbidelli, 2001), A and B have the form:

$$A = \frac{\beta}{3 - D}$$

$$B = \frac{2 - \beta}{3 - D}$$

where D is the fractal dimension and β is an auxiliary parameter defined as:

$$\beta = 1 + (2 + X)(1 - \alpha)$$

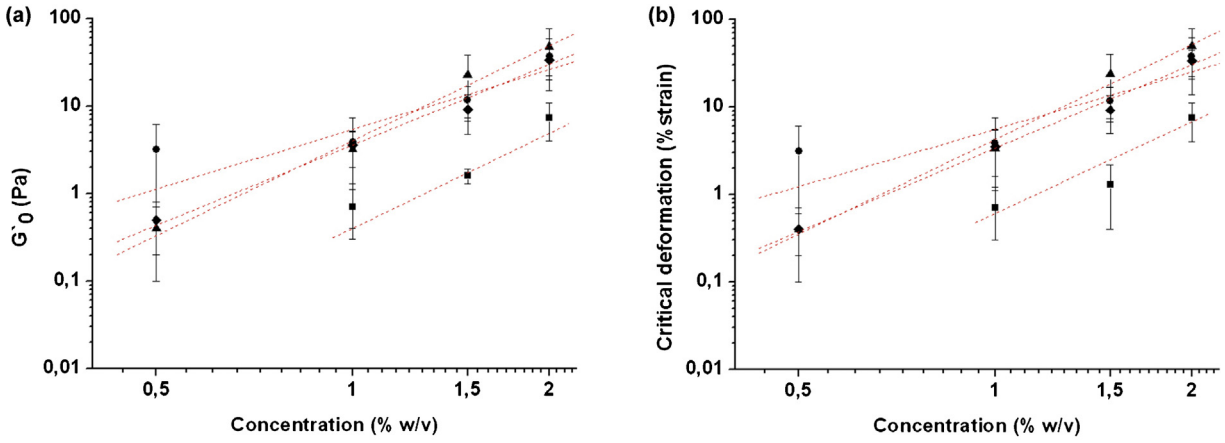

Fig. 5. (A) Elastic modulus plateau evolution and (B) critical deformation as a function of concentration of dispersion: CS + TPP (■), NP + Fe 1% (●), NP + Fe 3.2% (▲), and NP + Fe 5.6% (♦).

The exponent X represents the backbone fractal dimension or tortuosity of the network, whose value for a colloidal gel is in the range of 1.0–1.3 (Wu & Morbidelli, 2001). α is a constant in the range [0,1] which depends on the relation between the intra and the intermicroscopic elasticity which gives rise to the macroscopic elasticity in colloidal gels. $\alpha = 0$ corresponds to a strong-link regime where interfloc links are stronger than intrafloc links so that the gel elasticity is dominated by the intramicroscopic elasticity. On the other hand, $\alpha = 1$ corresponds to a weak-link regime where interfloc links are weaker than intrafloc links, that is, the gel elasticity is dominated by the intermicroscopic elasticity (Shih, Shih, Kim, Liu, & Aksay, 1990). According to the Wu and Morbidelli model (Wu & Morbidelli, 2001), intermediate regimes are obtained for values of α in the range $0 < \alpha < 1$. These intermediate regimes that are in between the weak-like and strong-like regime are more real leading to intermediate situations where both inter- and intrafloc links contribute to the overall elasticity of the gel.

As can be observed, data represented in Fig. 5 can be well fitted to a linear regression from which the slope is employed to determine the fractal dimension, D, and α constant. The results are summarized in Table 3.

Values corresponding to α are close to 1 in all cases which indicates that the samples are in the weak-like regime, that is, the interflocs links are weaker than intrafloc links. This implies that the macroscopic elasticity exhibited by the aqueous dispersions is due to the establishment of interactions between the individual chitosan NPs regardless the presence of magnetite. The fact that the interactions regime does not change with the magnetite concentration in aqueous dispersions of NP + Fe samples may be a consequence of the efficient encapsulation of magnetite inside the chitosan matrix.

Table 3
Summary of the results obtained by applying Wu and Morbidelli's scaling theory.

Sample	A	B	D	α	Regime
CS + TPP	6.2	5.9	2.8	0.9	Weak
NP + Fe 1.0%	3.4	3.3	2.7	0.9	Weak
NP + Fe 3.2%	5.3	5.3	2.8	1.0	Weak
NP + Fe 5.6%	4.4	4.7	2.7	1.0	Weak

A fractal dimension of ~2.8 is found for all samples indicating the occurrence of dense fractal flocs. Interestingly, no change in fractal dimension is observed with the addition of magnetite to the material in agreement with the weak-like regime observed for all the samples, and the predominant interactions between the chitosan matrixes of the different nanoparticles.

3.3. Cytotoxicity study

Fig. 6 shows the results corresponding to the Alamar Blue assay carried out for all the samples under study dispersed at different concentrations in water.

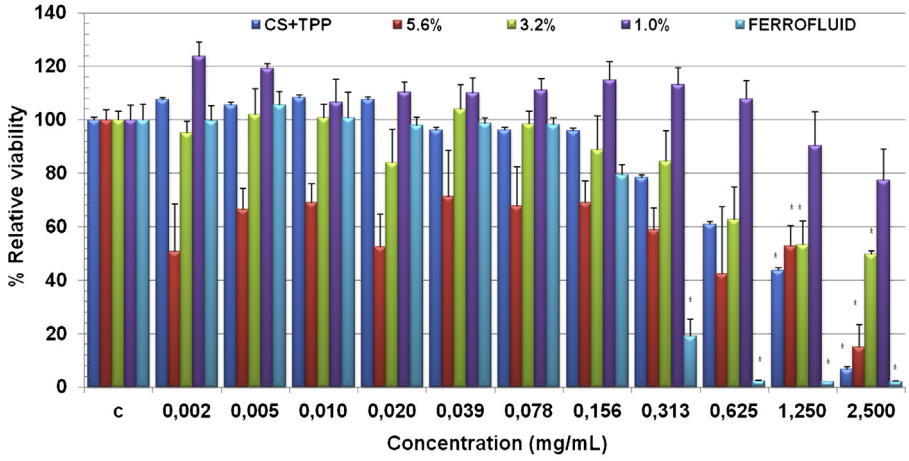

Fig. 6. Alamar Blue assay results for NP + Fe at different concentrations, for NPs and for the negative control, cells without treatment. All the results are shown as mean 8 S.D. asterisk (*) depicts a significant difference between the corresponding sample with respect to negative control ($P < 0.05$).

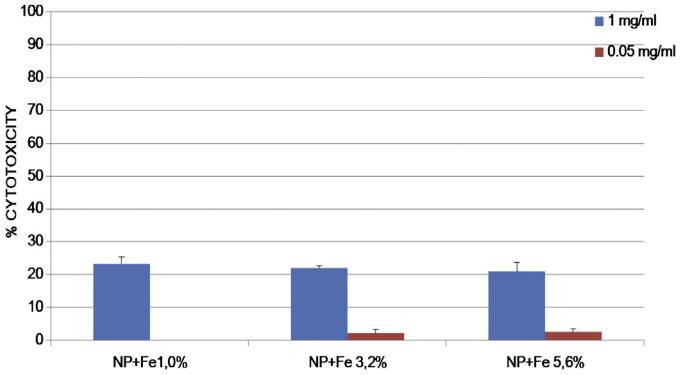

Fig. 7. Lactate dehydrogenase assay results for NP + Fe at different concentrations.

As can be observed, all the samples, including the ferrofluid exhibit a dose-dependent effect. At relatively high concentration of chitosan NPs (1.25 and 2.5 mg/mL), the cytotoxicity of systems NP + Fe 1.0% and NP + Fe 3.2% is very different, and the cell viability depends on the amount of ferrofluid noticeably. Even more, the cellular viability for those systems of NP + Fe 5.6% is compromised for a concentration of CS nanoparticles in the interval 0.625–2.50 mg/mL.

In order to establish the mechanism by which the NP + Fe samples tested with the AB assay gives rise to a decrease of the cellular viability, the test of lactate dehydrogenase (LDH) was performed. The LDH test allows to determine whether the plasma membrane is damaged. The results plotted in Fig. 7 indicate that the NP + Fe samples shows a cytotoxicity lower than 20% at the two concentrations tested (1.0 and 0.05 mg/mL). Therefore, cell death is not due to damage in the plasma membrane.

From these results, it can be concluded that the cytotoxic effect of the ferrofluid is decreased when it is encapsulated inside chitosan NPs. Therefore, NP + Fe samples do not compromise in vitro viability of this type of cells.

3.4. Remote heating

We furthermore evaluated the heating performance of NP + Fe nanoparticles when submitted to an alternating magnetic field (f = 580 kHz, H = 24 kA/m). Specifically, we extracted the specific power absorption (SPA) from the initial slope of the temperature vs time curves. The SPA of the colloids was determined from the temperature increase (ΔT) of a given mass of the constituent nanoparticles (m_{NP}) dispersed in a mass of liquid carrier (m_{LIQ}) during the time interval (Δt) of the experiment, *using the* expression (Lima et al., 2013):

$$SPA = \frac{P}{m_{NP}} = \frac{m_{LIQ}c_{LIQ} + m_{NP}c_{NP}}{m_{NP}}\left(\frac{\Delta T}{\Delta t}\right)$$

where c_{LIQ} and c_{NP} are the specific heat capacities of the liquid carrier and the nanoparticles, respectively. Due to the low concentration (around 1% wt.) of the magnetic material in the colloids we can use the approximation $m_{LIQ}c_{LIQ} + m_{NP}c_{NP} \approx m_{LIQ}c_{LIQ}$, so that the equation to calculate SPA becomes:

$$SPA = \frac{m_{LIQ}c_{LIQ}}{m_{NP}}\left(\frac{\Delta T}{\Delta t}\right)$$

Since the time dependence of temperature T is not linear, the slope of the $T(t)$ is also a function of time. This is usually due to heat losses of the experimental setup, and thus a criterion is needed in order to extract reproducible information from experiments. We have chosen the criterion of the maximum derivative for calculating our SPA values, since this criterion has two main advantages: first, the maximum slope $\Delta T/\Delta t$ happens during the first few second of the experiment, and therefore during this short time the heating process can be considered as adiabatic. Second, because it occurs during the first seconds after the magnetic field is turned on, the maximum slope is located at an absolute temperature close to room temperature, irrespective of the final SPA value. Consequently, all SPA values are estimated at nearly the same (room) temperatures.

Table 4
Specific power absorption of the samples under study.

Sample	$\Delta T/\Delta t$	Fe (mg/mL)	SPA (W/g)
FF	1.616	69.9	96.6
NP + Fe 1.0%	0.003	1.9	8.4
NP + Fe 3.2%	0.005	3.1	7.8
NP + Fe 5.6%	0.007	5.6	5.3

The SPA values for all NP + Fe samples are shown in Table 4 together with the data calculated for the pure ferrofluid.

As can be observed, there are significant differences between the value reported for the ferrofluid and the values corresponding to the NP + Fe samples. This is a consequence of the low amount of magnetic material of the NP + Fe nanoparticles, as the specific power is given in unit mass of the composite NPs. Therefore, these values could be improved if higher concentrations of Fe within the chitosan NPs can be encapsulated. In spite of the low SPA values reported here in comparison with the usually reported for pure ferrofluids, recent studies have outlined the capability of magnetic nanoparticles of inducing local damage in eukaryotic cells without increasing the macroscopic temperature, resulting in high percentages of cell death (Asin, Goya, Tres, & Ibarra, 2013; Asin, Ibarra, Tres, & Goya, 2012). It remains to be investigated whether similar mechanisms could be employed for intracellular drug release using magnetically loaded thermosensitive nanoparticles.

4. Conclusions

Iron oxide nanoparticles were encapsulated into chitosan NPs ionically crosslinked with TPP to yield magnetic core–shell chitosan nanoparticles with magnetite contents ranging from 1.0% to 5.6% (w/w). An increase in the size of the NP + Fe from 192 to 259 nm was observed as the magnetite content increased with respect to the chitosan NPs without magnetite (140 nm). A fractal analysis carried out on the results obtained from dynamic rheological experiments revealed the presence of interactions in between individual chitosan NPs and the absence of formation of aggregates independently from the magnetite content. Finally, aqueous dispersions of NP + Fe flow at high strains and recover the initial elastic properties as the strain rate diminishes which demonstrates the shear-thinning properties of these materials. Experiments on remote magnetic heating carried out on NP + Fe samples have revealed that aqueous dispersions (5.0%, w/v) undergo an increase of temperature when subjected to an alternating magnetic field. Therefore, NP + Fe samples can be considered as potential candidates for magnetic hyperthermia due to their good biocompatibility demonstrated in the cytotoxicity studies and their ability to heat when submitted to an AMF.

Supporting information

The strain sweeps carried out for all the samples under study at different concentrations of the dispersion in water.

Acknowledgements

The authors would like to express their appreciation to D. Gómez and M. Nieto for FESEM microscopy, to B. Sanz-Sagué for magnetic hyperthermia measurements, to C. Echeverría for helpful

discussions regarding the rheological analysis and to Laboratorio de Polímeros, Universidad Nacional de Costa Rica for their support in some of the results obtained. V. Zamora-Mora thanks CSIC for a JAE predoc fellowship, M. Fernández-Gutiérrez thanks CSIC for a JAE postdoc contract and R. Hernández thanks MEC for a Ramon y Cajal contract. Financial support from Fundación Domingo Martínez, L'ÓREAL-Unesco FWIS and MEC (MAT 2011-24797) is gratefully acknowledged.

Appendix A. Supplementary data

Supplementary data associated with this article can be found, in the online version, at http://dx.doi.org/10.1016/j.carbpol.2013.10.101.

References

Asin, L., Goya, G. F., Tres, A., & Ibarra, M. R. (2013). Induced cell toxicity originates dendritic cell death following magnetic hyperthermia treatment. *Cell Death Disease*, *4*, e596.

Asin, L., Ibarra, M. R., Tres, A., & Goya, G. F. (2012). Controlled cell death by magnetic hyperthermia: Effects of exposure time, field amplitude, and nanoparticle concentration. *Pharmaceutical Research*, *29*(5), 1319–1327.

Calvo, P., Remuñán-López, C., Vila-Jato, J. L., & Alonso, M. J. (1997). Novel hydrophilic chitosan-polyethylene oxide nanoparticles as protein carriers. *Journal of Applied Polymer Science*, *63*(1), 125–132.

Darder, M., Colilla, M., & Ruiz-Hitzky, E. (2003). Biopolymer-clay nanocomposites based on chitosan intercalated in montmorillonite. *Chemistry of Materials*, *15*(20), 3774–3780.

Darder, M., Colilla, M., & Ruiz-Hitzky, E. (2005). Chitosan-clay nanocomposites: Application as electrochemical sensors. *Applied Clay Science*, *28*(1–4), 199–208.

Dias, A. M. G. C., Hussain, A., Marcos, A. S., & Roque, A. C. A. (2011). A biotechnological perspective on the application of iron oxide magnetic colloids modified with polysaccharides. *Biotechnology Advances*, *29*(1), 142–155.

Doiron, A. L., Homan, K. A., Emelianov, S., & Brannon-Peppas, L. (2009). Poly(lactic-co-glycolic) acid as a carrier for imaging contrast agents. *Pharmaceutical Research*, *26*(3), 674.

Echeverria, C., López, D., & Mijangos, C. (2009). UCST responsive microgels of poly(acrylamide-acrylic acid) copolymers: Structure and viscoelastic properties. *Macromolecules*, *42*(22), 9118–9123.

Echeverria, C., Peppas, N. A., & Mijangos, C. (2012). Novel strategy for the determination of UCST-like microgels network structure: Effect on swelling behavior and rheology. *Soft Matter*, *8*(2), 337–346.

Gellermann, J., Hildebrandt, B., Issels, R., Ganter, H., Wlodarczyk, W., Budach, V., et al. (2006). Noninvasive magnetic resonance thermography of soft tissue sarcomas during regional hyperthermia. *Cancer*, *107*(6), 1373–1382.

Goya, G. F., Lima, E., Arelaro, A. D., Torres, T., Rechenberg, H. R., Rossi, L., et al. (2008). Magnetic hyperthermia with FeO nanoparticles: The influence of particle size on energy absorption. *IEEE Transactions on Magnetics*, *44*(11), 4444–4447.

Goycoolea, F. M., Lollo, G., Remuñán-López, C., Quaglia, F., & Alonso, M. J. (2009). Chitosan-alginate blended nanoparticles as carriers for the transmucosal delivery of macromolecules. *Biomacromolecules*, *10*(7), 1736–1743.

Gupta, A. K., & Gupta, M. (2005). Synthesis and surface engineering of iron oxide nanoparticles for biomedical applications. *Biomaterials*, *26*(18), 3995–4021.

Guvendiren, M., Lu, H. D., & Burdick, J. A. (2012). Shear-thinning hydrogels for biomedical applications. *Soft Matter*, *8*(2), 260–272.

Hernandez, R., Sacristán, J., Asi´n, L., Torres, T. E., Ibarra, M. R., Goya, G. F., et al. (2010). Magnetic hydrogels derived from polysaccharides with improved specific power absorption: Potential devices for remotely triggered drug delivery. *Journal of Physical Chemistry B*, *114*(37), 12002–12007.

Hernandez, R., Sacristan, J., Nogales, A., Fernandez, M., Ezquerra, T. A., & Mijangos, C. (2010). Structure and viscoelastic properties of hybrid ferrogels with iron oxide nanoparticles synthesized in situ. *Soft Matter*, *6*(16), 3910–3917.

Hernández, R., Zamora-Mora, V., Sibaja-Ballestero, M., Vega-Baudrit, J., López, D., & Mijangos, C. (2009). Influence of iron oxide nanoparticles on the rheological properties of hybrid chitosan ferrogels. *Journal of Colloid and Interface Science*, *339*(1), 53–59.

Jiang, D. -S., Long, S. -Y., Huang, J., Xiao, H. -Y., & Zhou, J. -Y. (2005). Immobilization of *Pycnoporus sanguineus* laccase on magnetic chitosan microspheres. *Biochemical Engineering Journal*, *25*(1), 15–23.

Jordan, A., Scholz, R., Maier-Hauff, K., Johannsen, M., Wust, P., Nadobny, J., et al. (2001). Presentation of a new magnetic field therapy system for the treatment of human solid tumors with magnetic fluid hyperthermia. *Journal of Magnetism and Magnetic Materials*, *225*(1–2), 118–126.

Jordan, A., Scholz, R., Wust, P., Fähling, H., & Roland, F. (1999). Magnetic fluid hyperthermia (MFH): Cancer treatment with AC magnetic field induced excitation of biocompatible superparamagnetic nanoparticles. *Journal of Magnetism and Magnetic Materials*, *201*(1–3), 413–419.

Kim, D. -H., Kim, K. -N., Kim, K. -M., & Lee, Y. -K. (2008). Targeting to carcinoma cells with chitosan- and starch-coated magnetic nanoparticles for magnetic hyperthermia. *Journal of Biomedical Materials Research Part A*, *88A*, 1–11.

Laurent, S., Dutz, S., Häfeli, U. O., & Mahmoudi, M. (2011). Magnetic fluid hyperthermia: Focus on superparamagnetic iron oxide nanoparticles. *Advances in Colloid and Interface Science*, *166*(1–2), 8–23.

Lawrie, G., Keen, I., Drew, B., Chandler-Temple, A., Rintoul, L., Fredericks, P., et al. (2007). Interactions between alginate and chitosan biopolymers characterized using FTIR and XPS. *Biomacromolecules*, *8*(8), 2533–2541.

Li, J., & Huang, Q. (2012). Rheological properties of chitosan–tripolyphosphate complexes: From suspensions to microgels. *Carbohydrate Polymers*, *87*(2), 1670–1677.

Li, Y., Huang, G., Zhang, X., Li, B., Chen, Y., Lu, T., et al. (2013). Magnetic hydrogels and their potential biomedical applications. *Advanced Functional Materials*, *23*(6), 660–672.

Lima, E., Jr., Torres, T. E., Rossi, L. M., Rechenberg, H. R., Berquo, T. S., Ibarra, A., et al. (2013). Size dependence of the magnetic relaxation and specific power absorption in iron oxide nanoparticles. *Journal of Nanoparticle Research*, *15*(5), 1–11.

Muzzarelli, R. A. (2011). Chitin nanostructures in living organisms. In N. S. Gupta (Ed.), *Chitin* (vol. 34) (pp. 1–34). Netherlands: Springer.

Muzzarelli, R. A. A., Boudrant, J., Meyer, D., Manno, N., Demarchis, M., & Paoletti, M. G. (2012). Current views on fungal chitin/chitosan, human chitinases, food preservation, glucans, pectins and inulin: A tribute to Henri Braconnot, precursor of the carbohydrate polymers science, on the chitin bicentennial. *Carbohydrate Polymers*, *87*(2), 995–1012.

Nicolás, P., Saleta, M., Troiani, H., Zysler, R., Lassalle, V., & Ferreira, M. L. (2013). Preparation of iron oxide nanoparticles stabilized with biomolecules: Experimental and mechanistic issues. *Acta Biomaterialia*, *9*(1), 4754–4762.

Pawlak, A., & Mucha, M. (2003). Thermogravimetric and FTIR studies of chitosan blends. *Thermochimica Acta*, *396*(1), 153–166.

Pham, K. N., Egelhaaf, S. U., Pusey, P. N., & Poon, W. C. K. (2004). Glasses in hard spheres with short-range attraction. *Physical Review E*, *69*(1), 011503.

Pham, K. N., Petekidis, G., Vlassopoulos, D., Egelhaaf, S. U., Pusey, P. N., & Poon, W. C. K. (2006). Yielding of colloidal glasses. *EPL (Europhysics Letters)*, *75*(4), 624.

Pham, K. N., Puertas, A. M., Bergenholtz, J., Egelhaaf, S. U., Moussaid, A., Pusey, P. N., et al. (2002). Multiple glassy states in a simple model system. *Science*, *296*(5565), 104–106.

Rodrigues, S., Costa, A. M. R. d., & Grenha, A. (2012). Chitosan/carrageenan nanoparticles: Effect of cross-linking with tripolyphosphate and charge ratios. *Carbohydrate Polymers*, *89*(1), 282–289.

Shih, W. -H., Shih, W. Y., Kim, S. -I., Liu, J., & Aksay, I. A. (1990). Scaling behavior of the elastic properties of colloidal gels. *Physical Review A*, *42*(8), 4772.

Ur-Rehman, T., Tavelin, S., & Gröbner, G. (2011). Chitosan in situ gelation for improved drug loading and retention in poloxamer 407 gels. *International Journal of Pharmaceutics*, *409*(1–2), 19–29.

Wu, Y., Hussain, M., & Fassihi, R. (2005). Development of a simple analytical methodology for determination of glucosamine release from modified release matrix tablets. *Journal of Pharmaceutical and Biomedical Analysis*, *38*(2), 263–269.

Wu, H., & Morbidelli, M. (2001). A model relating structure of colloidal gels to their elastic properties. *Langmuir*, *17*(4), 1030–1036.

Yan, C., Mackay, M. E., Czymmek, K., Nagarkar, R. P., Schneider, J. P., & Pochan, D. J. (2012). Injectable solid peptide hydrogel as a cell carrier: Effects of shear flow on hydrogels and cell payload. *Langmuir*, *28*(14), 6076–6087.

Zhang, L. -y., Zhu, X. -j., Sun, H. -w., Chi, G. -r., Xu, J. -x., & Sun, Y. -l. (2010). Control synthesis of magnetic Fe_3O_4–chitosan nanoparticles under UV irradiation in aqueous system. *Current Applied Physics*, *10*(3), 828–833.

Zhao, D.-L., Wang, X.-X., Zeng, X.-W., Xia, Q.-S., & Tang, J.-T. (2009). Preparation and inductive heating property of Fe_3O_4–chitosan composite nanoparticles in an AC magnetic field for localized hyperthermia. *Journal of Alloys and Compounds*, *477*(1–2), 739–743.

Zhi, J., Wang, Y., Lu, Y., Ma, J., & Luo, G. (2006). In situ preparation of magnetic chitosan/Fe_3O_4 composite nanoparticles in tiny pools of water-in-oil microemulsion. *Reactive and Functional Polymers*, *66*(12), 1552–1558.

Zhu, A., Yuan, L., & Liao, T. (2008). Suspension of Fe_3O_4 nanoparticles stabilized by chitosan and o-carboxymethylchitosan. *International Journal of Pharmaceutics*, *350*(1–2), 361–368.